ELSEVIER

Journal of Alloys and Compounds 330–332 (2002) 584–589

Journal of ALLOYS AND COMPOUNDS

www.elsevier.com/locate/jallcom

Synthesis and hydrogenation behavior of Mg–Ti–Ni–H systems by hydrogen-induced mechanical alloying

Tae-Whan Hong*, Young-Jig Kim

School of Metallurgical and Materials Engineering, SungKyunKwan University, 300 Chunchun-Dong, Jangan-Gu, Suwon, Kyungki-Do 440-746, South Korea

Abstract

Mg and Mg alloys are attractive hydrogen storage materials because of their lightweight and high absorption capacity. Their range of applications could be further extended if their hydrogenation properties and degradation behavior could be improved. The main emphasis of this study was to find an economic manufacturing method for Mg–Ti–Ni–H systems, and to investigate their hydrogenation properties. $(Mg_{10-x}Ti_x)$–10, 20 mass% Ni systems were prepared by hydrogen-induced mechanical alloying (HIMA) using Mg and Ni chips and sponge Ti. The particles synthesized were characterized by X-ray diffraction, and their morphologies were observed by means of scanning electron microscopy (SEM) with energy dispersive spectrometry (EDS). The absorbed hydrogen capacity (AHC) was measured by using thermogravimetry analysis (TGA) after HIMA. In addition, the crystal structures were analyzed in terms of their bright-/dark field images and the selected area diffraction pattern (SADP) of transmission electron microscopy (TEM). In order to examine hydrogenation behavior, a Sieverts type automatic pressure–composition–isotherm (PCI) apparatus was used and the experiments were performed at 423, 473, 523, 573, 623 and 673 K. The results of TGA reveal that the absorbed hydrogen contents are around 2.5 mass% for (Mg_9Ti_1)–10 mass% Ni. With increased Ni content, the absorbed hydrogen content decreases to 1.7 mass%, whereas the dehydriding starting temperatures are lowered by some 70–100 K. The results of PCI on (Mg_9Ti_1)–20 mass% Ni show that its hydrogen capacity is around 5.3 mass% and its reversible capacity and plateau pressure are also excellent at 523 and 573 K. In addition, the reaction enthalpy, $\Delta H_{D.plateau}$, is -30.6 ± 5.7 kJ/mol H_2.

Keywords: PCI; $\Delta H_{D.plateau}$; Hydrogen capacity; Absorbed hydrogen contents; Mg–Ti–Ni–H system

1. Introduction

Even though magnesium and magnesium alloys are attractive lightweight hydrogen absorbing materials, their hydrogen storage properties must be improved for practical applications. The improvement in their hydriding/dehydriding kinetics is especially important. Some studies have shown that combining multiphase magnesium with transition metals and intermetallic compounds could improve its hydrogenation kinetics. However, crystal structure modification of nanocrystalline structures with amorphous phases is also considered an effective method for improving the kinetic properties of the Mg and Mg alloys as well as for dealing with other problems related to those metals [1–5].

On the other hand, it is well known that titanium has a high hydrogen capacity and relatively good kinetics at high temperature. However, the synthesis of titanium hydrides is difficult and dangerous because these hydrides are generally manufactured by exposing metals to hydrogen gas at high temperatures and under convenient pressure [6,7].

The binary phase diagram of the Mg–Ti system shows that no intermetallic compound formed and the elements have negligible solubility for each other [8]. We expect to show by our study that using hydrogen-induced mechanical alloying (HIMA) can expand the solubility limits of the nano-/amorphous Mg and Ti alloys and improve their hydrogen kinetics for more economical applications.

2. Experimental details

2.1. Fabrication and characterization

Mg chips (99.93%), Ni chips (99.92%) and sponge Ti were used for HIMA. Mg and Ni chips were prepared by drilling without the cutting oil from ingots. The initial

*Corresponding author.

0925-8388/02/$ – see front matter
PII: S0925-8388(01)01507-9

mixtures (($Mg_{10-x}Ti_x$)–10, 20 mass% Ni, x=1 or 2, 8–12 g) were charged in an AISI 304 jar designed for high pressure operation and equipped with needle valves for evacuating air and introducing hydrogen gas. A 450-cc jar and 0.5-inch Cr steel balls (AKS) were used, and the balls-to-chips mass ratio (BCR) is 30:1. After evacuating air to 6.7 Pa by means of a rotary pump, the chips were processed by reactive mechanical alloying for 72 h under 2 MPa of high purity hydrogen gas (99.999%). The processing was done at 200 rpm and at ambient temperature using a planetary ball mill (Fritsch, pulverisette-5).

The HIMA particles were characterized by X-ray diffraction patterns (M18XHF-SRA diffractometer, Macscience, 1.5405 Å Cu Kα, 2°/min). The morphology of the particles was observed using scanning electron microscopy (SEM, JSM-35CF, Jeol) along with energy dispersing spectrometry (EDS, Tracor Northern Series III) and transmission electron microscopy (TEM, Hitachi H-9000-NA).

2.2. Evaluation of hydrogenation properties

In order to find the dehydrogenation starting temperature and hydrogen contents absorbed during HIMA, thermogravimetry analysis (TGA) was carried out under a pure argon atmosphere heated to 773 K at a rate of 1 K/min. For the evaluation of the hydriding/dehydriding behavior and the calculation of the reaction enthalpy on synthesized ($Mg_{10-x}Ti_x$)–10, 20 mass%Ni, pressure–composition–isotherm (PCI) measurements were carried out at 423, 473, 523, 573, 623 and 673 K without activation treatments.

3. Results and discussion

Fig. 1a shows the X-ray diffraction patterns in (Mg_9Ti_1) systems. As-received Mg_9Ti_1 patterns were broadened by the effects of nanocrystallization and/or amorphization. The patterns and background consisted of MgH_x and TiH_x mainly with unknown peaks. However, the intensities of MgH_x and TiH_x peaks decreased rapidly after alloying of additive nickel. The formation of binary hydrides is caused by the solubility limit of the Mg–Ti system. As a result of the effects of the added nickel, Mg–Ni and Ti–Ni intermetallic hydrides become more readily synthesized than binary hydrides, since the hydriding properties of intermetallic hydrides are superior to those of binary hydrides.

The trends shown in Fig. 1b for the Mg_8Ti_2 binary system are similar to those seen in Fig. 1a. However, in spite of increases in the amount of the nickel, TiH_x remained strong even in the patterns of the (Mg_8Ti_2)–20 mass% Ni system. Moreover, the intensity of the unknown peaks weakened due to increases in the peaks of Mg–Ni and Ti–Ni hydrides. To sum up the results of XRD, even if the possibility of synthesis of ($Mg_{10-x}Ti_x$)–10, 20 mass% Ni synthesis is confirmed by HIMA, with increases in additive nickel it is thought that the phases of particles

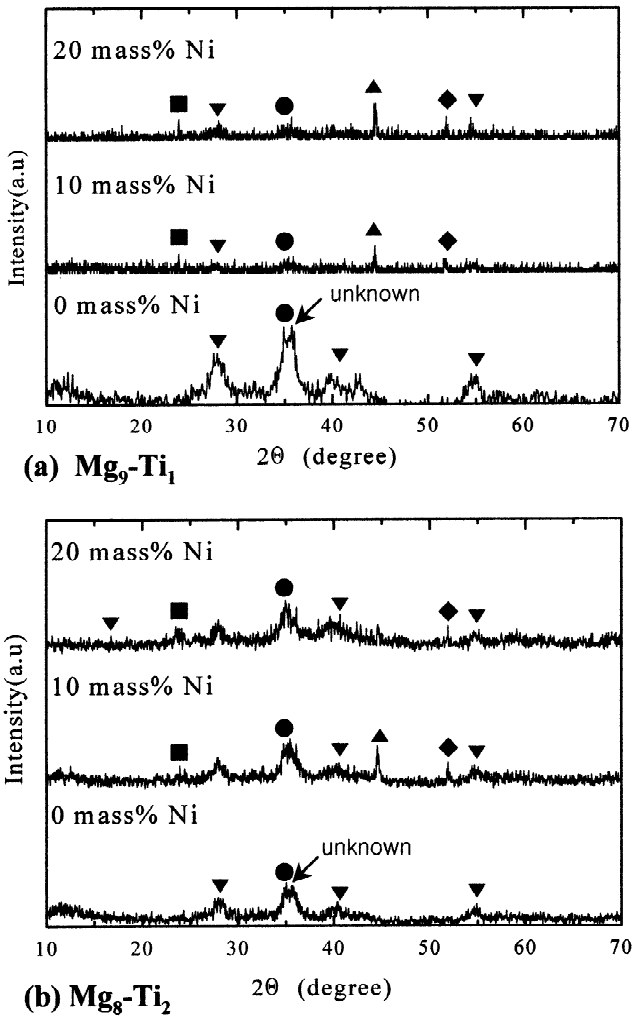

Fig. 1. Results of XRD patterns with respect to additive Ni after 72 h HIMA (■, Mg_2NiH; ▼, MgH_x; ●, TiH_x; ♦, Ni; ▲, Ti_2NiH_x).

synthesized in ($Mg_{10-x}Ti_x$)–10, 20 mass% Ni systems are separated by Mg–Ni and Ti–Ni intermetallic hydrides. It is especially noteworthy that the peaks of Ti–Ni hydrides are greater in intensity than those of Mg–Ni hydrides.

Fig. 2 shows the morphology of synthesized particles of (Mg_9Ti_1) and (Mg_9Ti_1)–20 mass% Ni. The average particle sizes of (Mg_9Ti_1) are measured at around 0.1–0.5 μm, and those of (Mg_9Ti_1)–20 mass% Ni are observed to be around 0.5–15 μm. However, some agglomerated particles composed of fine particles appeared. The effects of additive nickels revealed that the physical properties of nickel (e.g. ductility) led to the formation of large agglomerated particles. In addition, the agglomerated Ti–Ni particles are larger than Mg–Ni ones.

Fig. 3a shows the bright field images and related selected area diffraction patterns (SADP) of (Mg_9Ti_1)–10 mass% Ni. The bright field images are composed of nanocrystalline (less than ~15 nm) in an amorphous phase, and it is distinguished between dark gray (Mg–Ni rich phase) and bright gray (Ti–Ni rich phase) regions. Further-

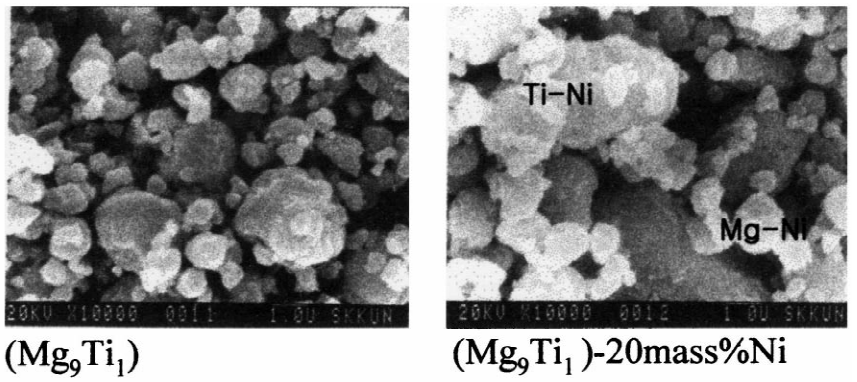

Fig. 2. Morphology of synthesized particles with respect to additive Ni.

more, SADP revealed that the patterns achieved a continuous and broadening ring that included unknown spots. Such trends of ring patterns proved that the phase formed a nano-/amorphous structure with unknown regions. These results of TEM are similar to those found in other alloy systems.

Fig. 4 shows that the TGA obtained for (Mg_9Ti_1)–10 mass% Ni–H and (Mg_9Ti_1)–20 mass% Ni–H samples.

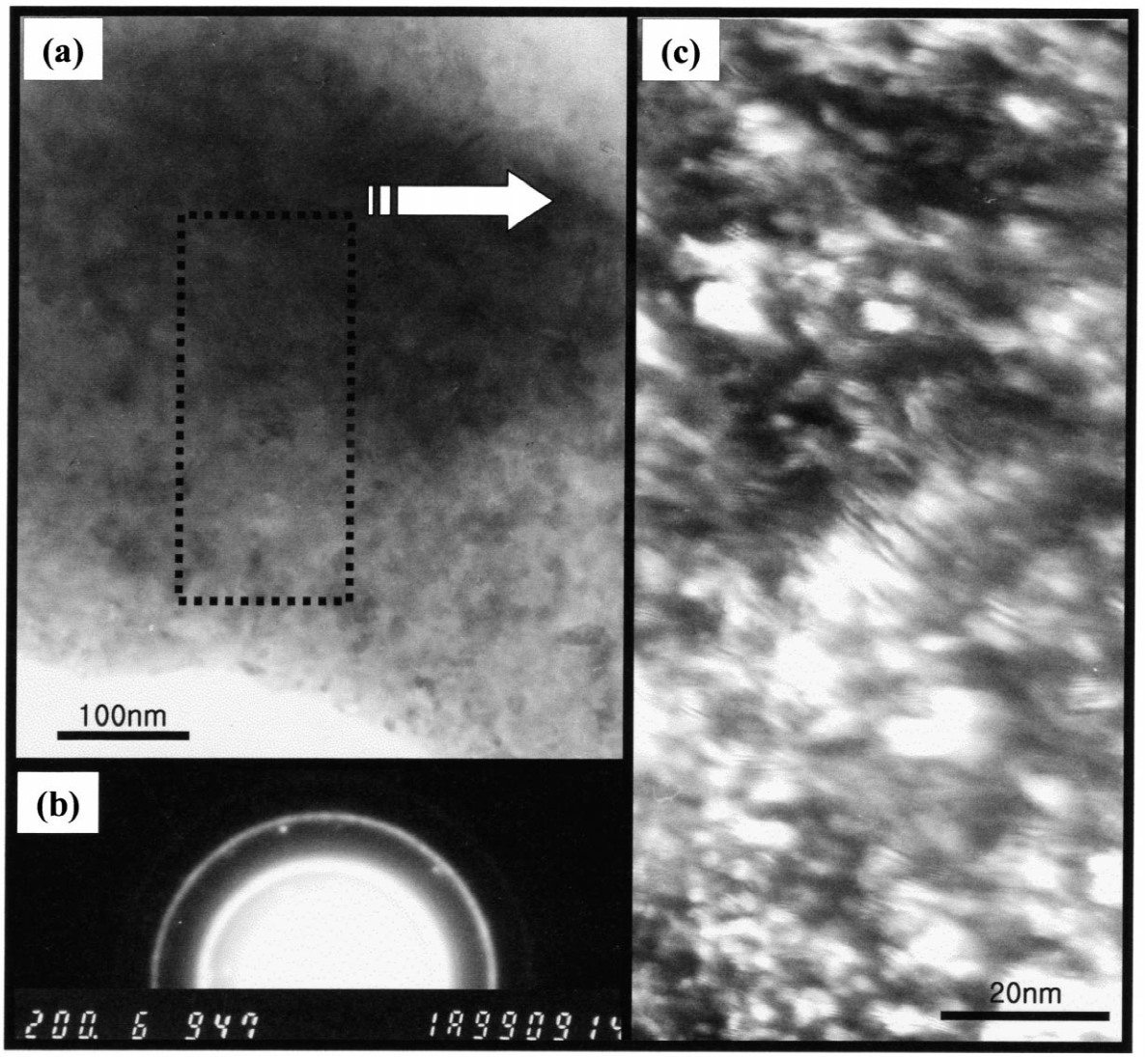

Fig. 3. (a) TEM bright field image, (b) SAD pattern and (c) dark field image of the (Mg_9Ti_1)–10 mass% Ni alloy.

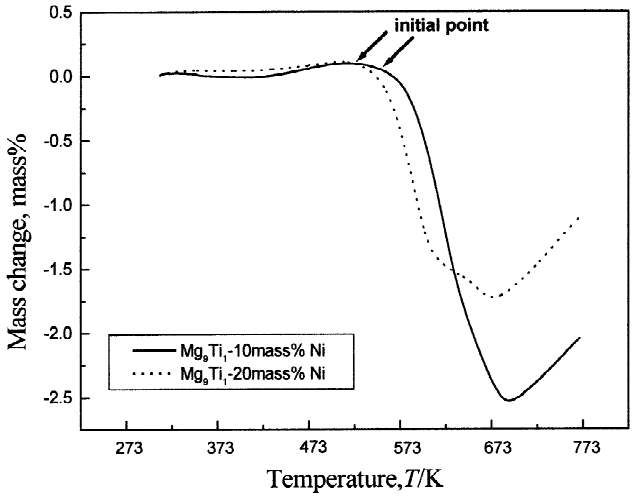

Fig. 4. Results of TGA on (Mg_9Ti_1)–10 mass% Ni–H and (Mg_9Ti_1)–20 mass% Ni–H samples system.

TGA revealed that AHC via HIMA reached around 2.5 and 1.7 mass% for (Mg_9Ti_1)–10 mass% Ni–H, (Mg_9Ti_1)–20 mass% Ni–H, respectively. With increase of the nickel content, AHC is slightly decreased, whereas the dehydriding starting temperature (the reaction initial points indicated in the figure) is lowered by around 70–100 K. Because of the catalytic behavior of nickel, the hydrogen capacity decreased while dehydriding kinetics improved [9].

Fig. 5 shows the hydriding/dehydriding behavior of specimens at 523 K. In the field of hydriding behavior, the majority of profiles revealed that hydrogen capacities reached around 4.3–5.8 mass% and reversible capacities attained were over 3.0 mass%. However, plateau levels were raised by two steps through the effects of Mg–Ni and Ti–Ni intermetallic hydrides except in the case of the $(Mg_{10-x}Ti_x)$ system. With regard to dehydriding behavior, the rest curves retained hydrogen around 0.4–1.8 mass%, except in the case of (Mg_9Ti_1)–20 mass% Ni and (Mg_8Ti_2)–10 mass% Ni alloys. In addition, the plateau pressure appeared below 0.03 MPa and was raised for non-equilibrium reactions.

Fig. 6 shows the hydrogenation behavior of $(Mg_{10-x}Ti_x)$–10, 20 mass% Ni systems at 573 K. Even though the operating temperature is high, the hydriding/dehydriding reactions have a favorable profile except in the case of (Mg_9Ti_1)–10 mass% Ni and (Mg_8Ti_2)–20 mass% Ni alloys. It is especially important that the plateau did not

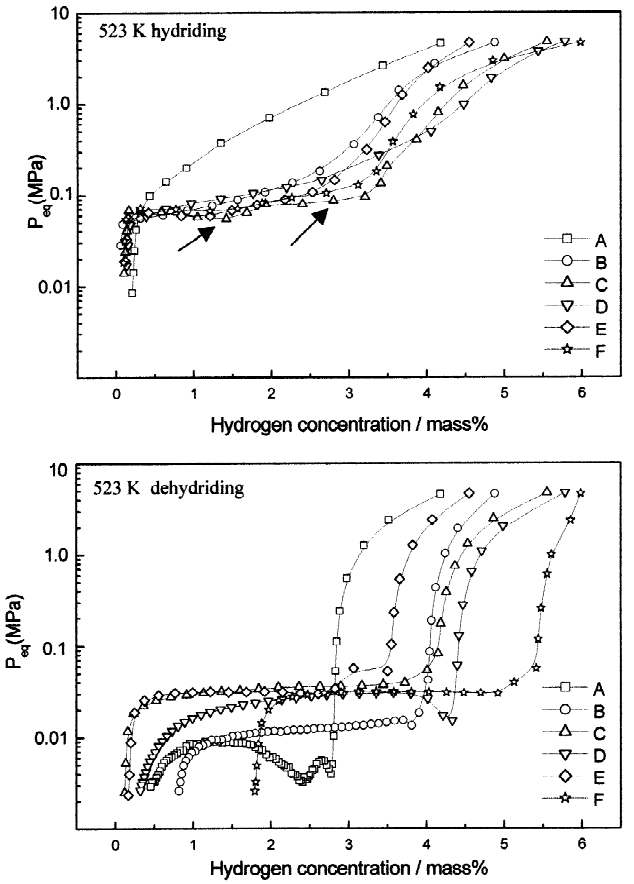

Fig. 5. Pressure–composition–isotherm curves on Mg_9Ti_1 (A), Mg_9Ti_1–10 mass% Ni (B), Mg_9Ti_1–20 mass% Ni (C), Mg_8Ti_2 (D), Mg_8Ti_2–10 mass% Ni (E) and Mg_8Ti_2–20 mass% Ni (F) at 523 K.

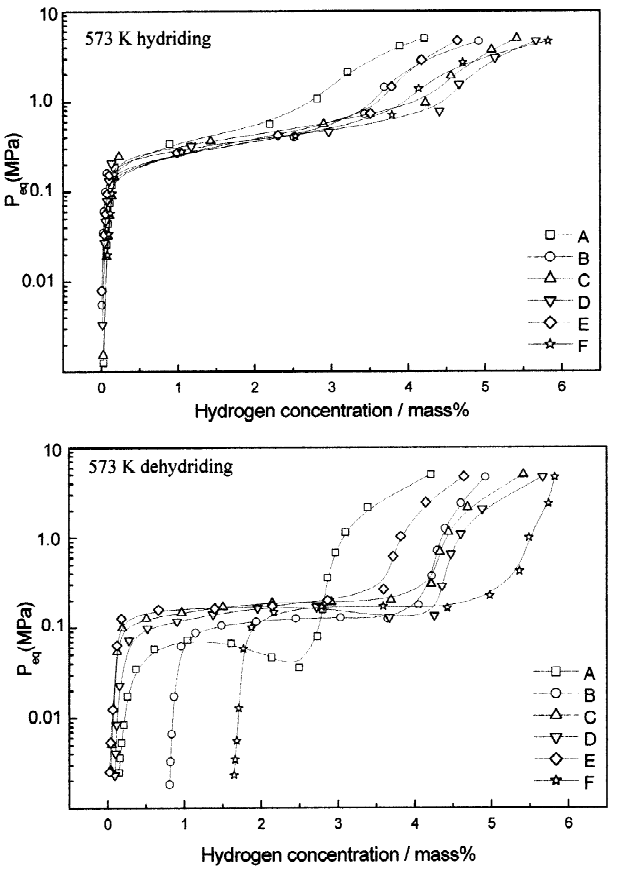

Fig. 6. Pressure–composition–isotherm curves on Mg_9Ti_1 (A), Mg_9Ti_1–10 mass% Ni (B), Mg_9Ti_1–20 mass% Ni (C), Mg_8Ti_2 (D), Mg_8Ti_2–10 mass% Ni (E) and Mg_8Ti_2–20 mass% Ni (F) at 573 K.

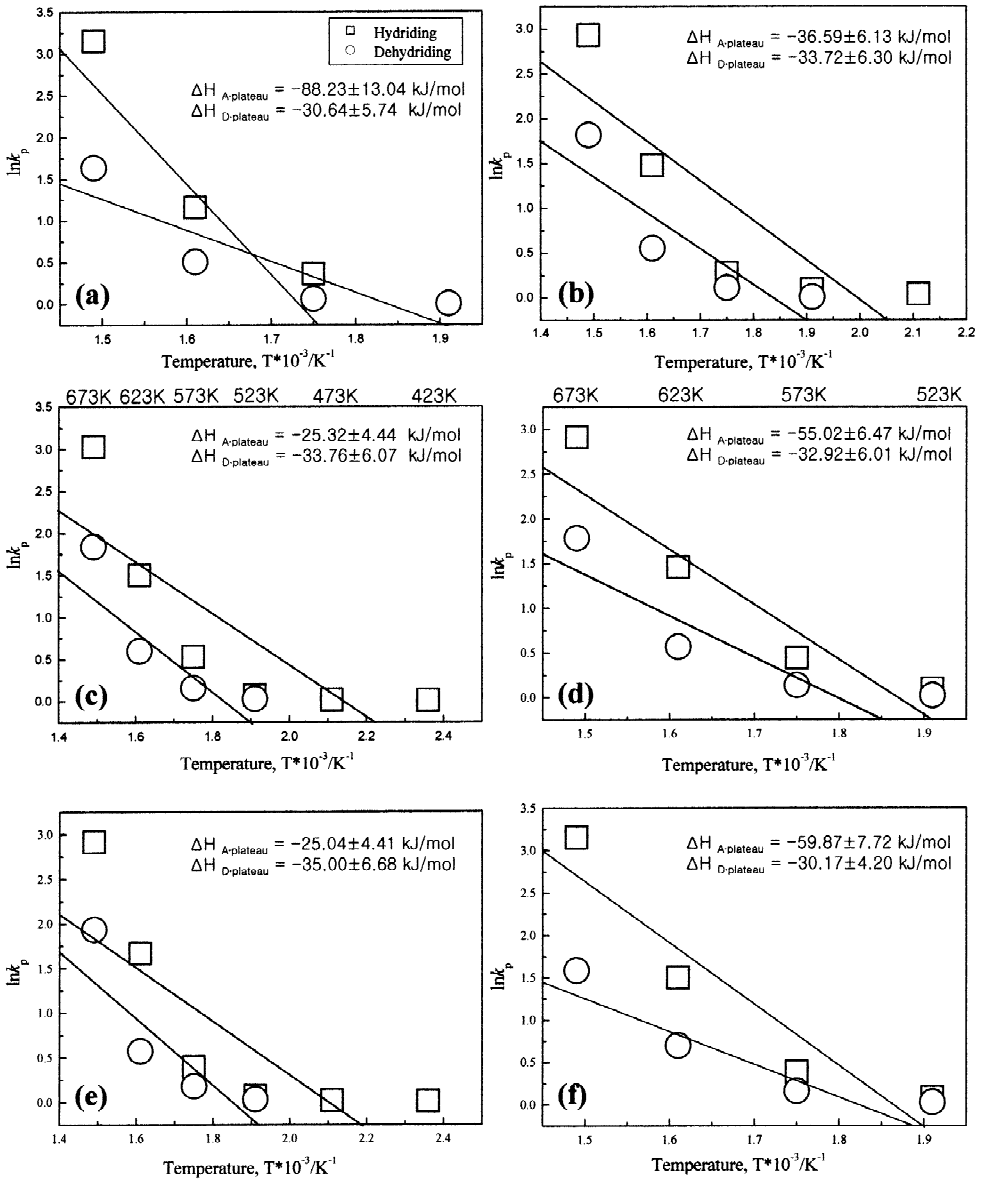

Fig. 7. The van't Hoff plots related mean plateau pressure on (a) Mg_9Ti_1, (b) Mg_9Ti_1–10 mass% Ni, (c) Mg_9Ti_1–20 mass% Ni, (d) Mg_8Ti_2, (e) Mg_8Ti_2–10 mass% Ni and (f) Mg_8Ti_2–20 mass% Ni.

show the two steps because of the effects of high temperature. Also, the plateau pressures of dehydriding behavior in half of the alloys were indicated to be over 0.1 MPa. In those cases, hydrogen capacity reached between about 4.5 and 5.5 mass% for (Mg_8Ti_2)–10 mass% Ni and (Mg_9Ti_1)–20 mass% Ni, respectively.

Fig. 7 shows the van't Hoff plots that related the plateau pressure on PCI measurements. The hydriding plots of Fig. 7c,e are obtained by calculating the mean plateau pressure from 423 to 673 K, and reaction enthalpies for $\Delta H_{\text{A.plateau}}$, are calculated to be around -25.3 ± 4.4 and -25.0 ± 4.4 kJ/mol H_2, respectively. However, the plots of dehydriding reactions are illustrated after 523 K, and $\Delta H_{\text{D.plateau}}$ are calculated to be around -30.1 ± 4.2 to -35.0 ± 6.6 kJ/mol H_2 from 523 to 673 K. Putting evaluations of hydrogenation properties together (Mg_9Ti_1)–20 mass% Ni alloys are the best of the materials examined in this study.

4. Conclusions

$(Mg_{10-x}Ti_x)$–10, 20 mass% Ni systems composed of nanocrystalline and amorphous phases have been synthesized successfully by means of hydrogen-induced mechanical alloying using Mg and Ni chips and sponge Ti. Additive nickel mainly affected hydrogenation properties due to the formation of Mg–Ni and Ti–Ni intermetallic hydrides, and the dual phase led to a two-step plateau below 523 K in the cases of most specimens. Titanium contributed greatly to improving factors on hydrogen

capacities, plateau pressure and kinetics at high temperature ranges. However, the dehydrogenation properties of all specimens have to be improved for operation at low temperatures.

References

[1] L. Schlapbach (Ed.), Hydrogen Intermetallic Compounds II, Springer, Berlin, 1992, p. 178.
[2] L. Zaluski, A. Zaluska, J.O. Ström-Olsen, J. Alloys Comp. 217 (1995) 245.
[3] F.J. Liu, S. Suda, J. Alloys Comp. 231 (1995) 392.
[4] K.J. Gross, D. Chartouni, E. Leroy, A. Züttel, L. Schlapbach, J. Alloys Comp. 269 (1998) 259.
[5] T.W. Hong, S.K. Kim, G.S. Park, Y.J. Kim, Mater. Trans., JIM 41 (2000) 393.
[6] L. Lewkowicz, in: F.A. Lewis, A. Aladjem (Eds.), Hydrogen Metal Systems I, Scitec, Switzerland, 1996, p. 239.
[7] J.-L. Bobet, C. Even, Y. Nakamura, E. Akiba, B. Darriet, J. Alloys Comp. 298 (2000) 279.
[8] T.B. Massalski (Ed.), Binary Alloy Phase Diagrams, ASM, Ohio, U.S.A., 1986, p. 1555.
[9] J. Hout, E. Akiba, T. Takada, J. Alloys Comp. 231 (1995) 815.